Academic Journal of Applied Sciences
ISSN: 3105-0549 (Print), ISSN: 3105-0557 (Online) | Vol. 1, No. 1, 2026

Research on Stereo Matching Method for Ultra-Thin Strip-Shaped Materials of Power Battery Covers Based on Multi-Algorithm Fusion

Xingran Luo *, Yinghua Liao, Ruifeng Yang

Sichuan University of Science & Eegineering, Yibin 644000, China

*** Corresponding author**

Abstract: To address the problems of incomplete feature extraction and high mismatch rates in traditional stereo matching of ultra-thin strip materials for power battery top covers, a stereo matching method integrating edge enhancement and robust matching is proposed. First, the Canny edge detection algorithm is employed to accurately extract the edge contours of the power battery top cover, suppressing image noise while ensuring edge continuity and local feature integrity. Then, the SIFT algorithm is used to achieve cross-scale matching of feature points between the left and right images, enhancing robustness against deformation and rotation. Finally, the RANSAC algorithm is applied to eliminate mismatched points and construct a high-precision stereo matching model. Experimental results show that compared with the traditional NCC algorithm, the proposed stereo matching method improves the matching rate by 2.7% and reduces the matching time by 12.4 seconds; compared with the SGM algorithm, it increases the matching rate by 4.68% and shortens the processing time by 9 seconds, significantly optimizing the stereo matching performance for ultra-thin strip materials.

Keywords: Power battery top cover; Ultra-thin strip material; Stereo matching; Canny edge detection; SIFT algorithm; RANSAC algorithm.

1. Introduction

With the rapid development of the new energy vehicle industry, the quality and performance of power batteries have garnered increasing attention. As a critical component of the power battery, the production quality of the power battery cover directly affects the safety and reliability of the battery [1]. During the production process of the cover, quality inspection is of paramount importance. Traditional inspection methods for power battery covers primarily include manual visual inspection and non-contact inspection. Manual visual inspection [2] suffers from low efficiency and low accuracy, and is easily influenced by subjective factors, leading to poor consistency of inspection results and a high rate of missed detections. Non-contact inspection methods [3-5] mainly include X-ray inspection, ultrasonic inspection, and computer vision inspection. X-ray and ultrasonic inspection can penetrate materials to detect internal defects, but they pose issues such as radiation safety risks and high costs. Computer vision inspection, on the other hand, does not require contact with the test object and offers advantages such as high efficiency and low cost. The above methods are suitable for small-batch sampling inspection and require specialized personnel to manually inspect the sampled specimens using dedicated equipment, making them incapable of meeting the real-time, full-inspection requirements of high-reliability, high-safety power battery production lines.

In recent years, with the advancement of computer vision technology, binocular vision measurement systems have provided a new approach for power battery cover inspection. Wang Wei et al [6]. proposed a point cloud-based local flatness detection method that uses clustering and template matching algorithms for point cloud alignment, significantly reducing computation time while achieving high alignment accuracy. Binocular vision technology can acquire three-dimensional information of objects, offering a new avenue for material inspection. Toki et al [7]. proposed a binocular stereo vision method utilizing machine learning techniques, employing two machine learning algorithms, Support Vector Machine and Random Forest, for stereo matching and pedestrian detection. Ismail et al [8]. developed a non-contact high-precision measurement system based on binocular stereo vision technology, accurately obtaining three-dimensional data of the detection target. To detect surface defects such as undercuts and depressions in laser-welded aluminum alloy thin sheets, Zhang Chen et al [9]. developed a deep learning-based online defect monitoring system for rapid measurement of defect dimensions. Addressing the limitations of traditional manual measurement of sheet dimensions, such as low precision, heavy workload, and susceptibility to surface damage, Wang Haomeng et al [10]. designed a sheet dimension vision measurement system based on binocular vision technology. This system uses a region-growing algorithm combined with dilation and erosion operations to extract the sheet surface contour, and calculates the three-dimensional coordinates of points on the contour based on the principle of triangulation, thereby achieving high-precision dimension measurement of the sheet.

The above studies provide new stereo matching methods and insights for ultra-thin strip-shaped materials. However, due to the unique shape and optical characteristics of such materials, traditional stereo matching methods struggle to meet the high-precision inspection requirements. Therefore, this paper proposes a "three-level stereo matching optimization method" (edge detection — feature matching — robust optimization) suitable for ultra-thin strip-shaped materials for power battery covers. First, an improved Canny edge detection algorithm is used to accurately extract the contour of the power battery cover. Then, the feature point-based SIFT (Scale-Invariant Feature Transform) algorithm is employed to enhance matching accuracy. Finally, the RANSAC (Random Sample Consensus) algorithm is applied to eliminate mismatched points in the model, yielding high-precision stereo matching results.

2. Existing Problems in Traditional Stereo Matching

As shown in Figure 1, the power battery cover assembly is mainly composed of components such as the cover plate, explosion-proof valve, and injection-molded terminal, with dimensions of 173 mm × 53 mm and a thickness of 2 mm. Its function is to seal the top of the battery cell, ensuring isolation between the interior of the battery and the external environment, while providing necessary electrical connections and safety protection[11].

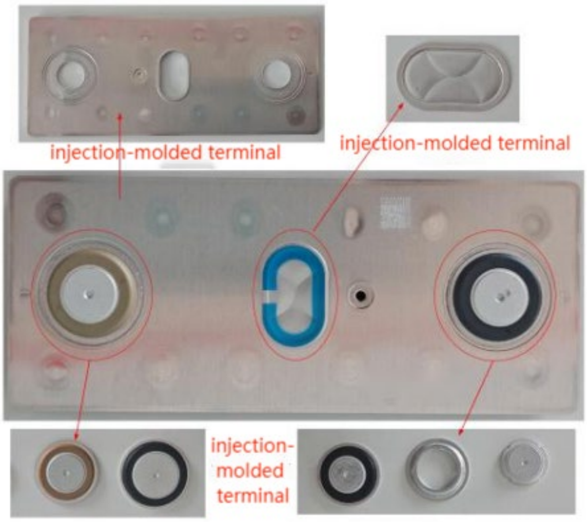

Figure 1. Power battery top cover assembly

From the composition and materials of the power battery cover, it can be seen that its structure is complex and its shape is unique. Therefore, ultra-thin strip-shaped materials such as the power battery cover often present the following problems in traditional stereo matching[12]:

(1) Loss of geometric features

The width of ultra-thin materials may occupy only a few pixels (or even sub-pixels), making it difficult for local windows (e.g., SAD, Census) to extract effective texture, and the disparity calculation is easily overwhelmed by background pixels.

(2) Edge aliasing and jagging effects

The edges of thin materials exhibit jagging due to pixel discretization, resulting in discontinuous disparity jumps at edges and making the matching cost function (e.g., NCC) sensitive to sub-pixel offsets.

(3) Highly reflective or transparent materials

Surfaces such as metal wires and glass fibers are prone to specular reflection or transmission: there is a significant brightness difference between the left and right views (e.g., one side is reflective while the other side is invisible), rendering traditional intensity-based matching (e.g., SSD) ineffective.

(4) Occlusion and fragmentation

Sleder objects may be partially occluded: mismatches occur in fragmented regions (e.g., background pixel filling), making it difficult to maintain continuity (e.g., failure of path aggregation in SGM).

3. Three-Stage Stereo Matching Optimization Method

The stereo matching process adopted in this paper is shown in Figure 2. It includes: image acquisition, camera calibration, image rectification, target contour extraction, feature point matching, and mismatching removal.

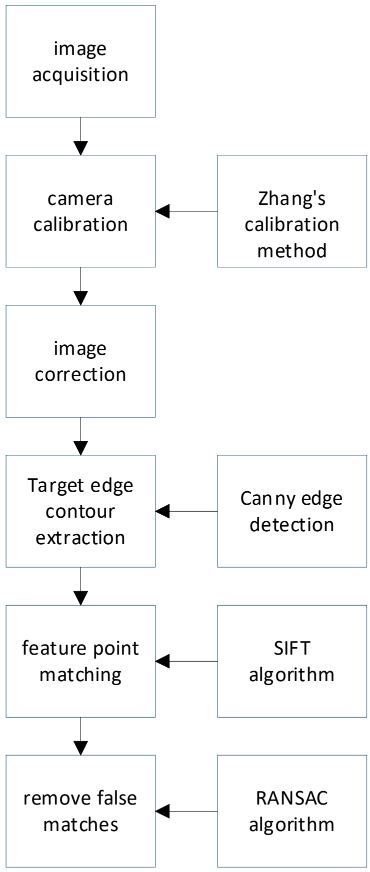

Figure 2. Stereo Matching Process

Since there may be differences in the positions and parameters of the two cameras, camera calibration is required to accurately calculate the three-dimensional information of the object. The purpose of camera calibration is to determine the intrinsic parameters of each camera (such as focal length, principal point position, distortion coefficients, etc.) and extrinsic parameters (such as rotation matrix and translation vector, which describe the relative position and orientation relationship between the cameras). The calibration method used in this experiment is Zhang Zhengyous calibration method [13]. The selected calibration board pattern is 8 × 6, with a grid square side length of 15 mm and an accuracy of ±0.01 mm. Calibration was performed using the MATLAB calibration toolbox, and the calibration parameters are shown in Table 1.

Table 1. Binocular stereo vision calibration results

	Left camera
internal reference	$\begin{bmatrix} 412.2234 & 0 & 0 \\ 0 & 412.8374 & 0 \\ 415.4662 & 242.0941 & 1 \end{bmatrix}$
distortion coefficient	$K_1 = 0.0246$, $K_2 = -0.0453$ $P_1 = 0.0015$, $P2 = -0.0092$

	Right camera
internal reference	$\begin{bmatrix} 412.0311 & 0 & 0 \\ 0 & 413.1630 & 0 \\ 412.3417 & 241.6143 & 1 \end{bmatrix}$
distortion coefficient	$K_1 = 0.0143$, $K_2 = 0.0179$ $P_1 = 0.0020$, $P2 = -0.0114$

	Left camera	Right camera
Rotation matrix R	$\begin{bmatrix} 1 & 3.0558 & -0.0073 \\ -3.1780 & 1 & -0.0017 \\ 0.0073 & 0.0017 & 1 \end{bmatrix}$	
translation vector t	$\begin{bmatrix} -56.9493 & -0.2354 & 1.6191 \end{bmatrix}$	

3.1. Edge Contour Extraction—Canny Detection Algorithm

To address issues such as image noise interference and loss of edge continuity during the matching process for ultra-thin strip-shaped materials like power battery covers, the Canny edge detection algorithm is used to extract the edge contour. The Canny algorithm is a multi-stage edge detection algorithm based on optimal detection criteria, designed to effectively suppress noise while maintaining edge continuity. By processing the image with the Canny operator, the edge information of the material can be effectively detected while suppressing noise interference [14]. The key steps of this algorithm [15] include: Gaussian filtering for noise reduction, calculating gradient magnitude and direction, non-maximum suppression, and dual-threshold detection. The Canny algorithm process is shown in Figure 3.

To reduce noise while preserving edge information, a convolution operation is performed using a two-dimensional Gaussian kernel with good noise reduction performance. The Gaussian filter, as a linear filter, is obtained by sampling a two-dimensional Gaussian function followed by normalization. In the Canny operator, the two-dimensional Gaussian function used is expressed in Equations (1) and (2). By applying this filter, it is possible to suppress noise while retaining the edge features of the image, providing a more accurate foundation for subsequent edge detection. Here, (x, y) are the coordinates in the filter kernel, and σ is the standard deviation of the Gaussian distribution, which controls the smoothing degree of the Gaussian filter. The larger the σ, the smoother the filtered image.

$$G(x, y, \sigma) = \frac{1}{2\pi\sigma^2} e^{-\frac{x^2+y^2}{2\sigma^2}} \tag{1}$$

$$S = I * G \tag{2}$$

Where:

G is the Gaussian filter;

I is the convolutional image to be detected;

* denotes the convolution operation;

S is the smoothed image.

Assuming the normal direction of a certain edge is θ, the components Gx and Gy of the pixel point gradient on this edge in the x and y directions are given by Equations (3) and (4):

$$G_x = \frac{S(x+1, y) - S(x-1, y)}{2} \tag{3}$$

$$G_y = \frac{S(1, y+1) - S(x, y-1)}{2} \tag{4}$$

The gradient magnitude M and direction θ of the pixel point are then given by Equations (5) and (6), respectively:

$$M = \sqrt{G_x^2 + G_y^2} \tag{5}$$

$$\theta = \arctan\left(\frac{G_y}{G_x}\right) \tag{6}$$

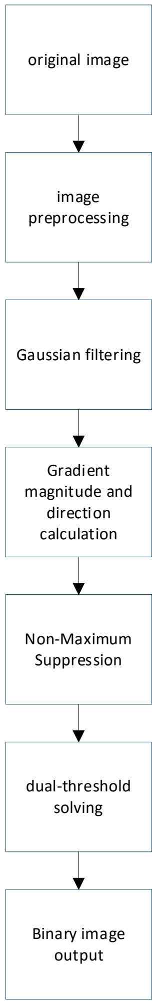

Figure 3. Flowchart of Canny algorithm

After calculating the gradient magnitude and direction, non-maximum suppression is applied to the gradient magnitude. The purpose is to find local maxima along the gradient direction and set the gradient magnitudes of other non-maximum points to zero, thereby thinning the edges.

3.2. Cross-Scale Feature Matching—SIFT Algorithm

To address issues such as non-uniform deformation (e.g., local bending) and out-of-plane rotation (tilt) of ultra-thin materials, representative feature points on the contour, such as points with significant curvature changes and endpoints, are selected after contour extraction. The SIFT algorithm is a feature extraction algorithm that maintains stability across different scales and rotations, exhibiting robustness to scale changes, rotation, occlusion, and viewpoint variations. However, due to its computational steps involving multi-scale space construction, feature extraction, and descriptor generation, it incurs a relatively high computational cost [16-

17]. The SIFT (Scale-Invariant Feature Transform) algorithm is used to match feature points between the left and right images, establishing preliminary correspondences. Although the SIFT algorithm is computationally intensive, it provides reliable matching results for material images with certain rotations and scale variations[18]. The SIFT algorithm process is shown in Figure 4.

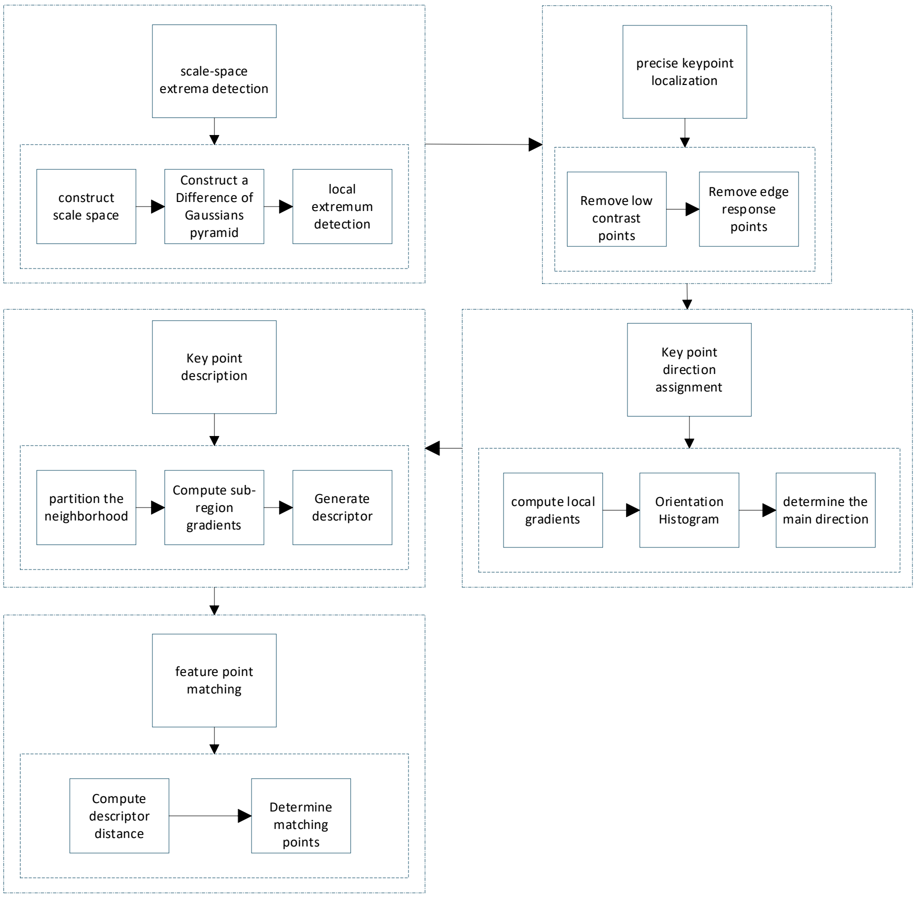

Figure 4. SIFT algorithm flowchart

The calculation formulas for the gradient magnitude m(x,y) and orientation θ(x,y) are given by Equations (7) and (8), respectively:

$$m(x,y)=\sqrt{(L(x+1,y)-L(x-1,y)^2+L(x,y+1)-L(x,y-1)^2)} \tag{7}$$

$$\theta(x,y)=\arctan\frac{L(x,y+1)-L(x,y-1)}{L(x+1,y)-L(x-1,y)} \tag{8}$$

Where L(x,y) is the Gaussian-blurred image at the scale where the keypoint is located.

3.3. Mismatch Elimination—RANSAC Algorithm

Due to issues such as possible discontinuities and noise at the edges of ultra-thin strip-shaped materials, mismatches may occur in the matching results. RANSAC is a robust model fitting algorithm [19], widely used in data containing noise and outliers. Its core concept is to estimate model parameters through multiple random samplings and select the optimal fit. To improve matching reliability, the RANSAC (Random Sample Consensus) algorithm is used to filter the matching point pairs. This algorithm randomly selects sample points, fits a model, and calculates the support of other points for the model, thereby eliminating mismatched points that do not conform to the model. After processing with the RANSAC algorithm, more accurate stereo matching results can be obtained.

Basic Concept of the RANSAC Algorithm [19]: Randomly select a minimal sample set from the data (e.g., 2 points for fitting a line, 3 points for a plane) and compute the model parameters. Use these parameters to classify all data into "inliers" (data conforming to the model) and "outliers" (anomalies that do not conform). Through iterative optimization, the model with the largest number of inliers is selected as the final result. The RANSAC algorithm process is shown in Figure 5.

The specific steps are as follows:

(1) Parameter Initialization: Set parameters for the RANSAC algorithm, such as the number of iterations, inlier threshold, and minimum number of inliers.

(2) Iteration Start: Enter the iterative loop of RANSAC.

(3) Random Sampling: Randomly select the minimum number of point pairs from the initial set of matching point pairs to compute the model parameters (e.g., the fundamental matrix).

(4) Model Calculation: Compute the corresponding model (e.g., fundamental matrix) based on the randomly selected point pairs.

(5) Inlier Screening: For all matching point pairs, calculate the error with respect to the current model (e.g., epipolar geometry error). If the error is less than the inlier threshold, the point pair is classified as an inlier.

(6) Model Evaluation: Count the number of inliers corresponding to the current model. If the number of inliers exceeds the minimum required number and is greater than the previously recorded maximum number of inliers, update the optimal model and the maximum number of inliers.

(7) Iteration Termination Judgment: Determine whether the preset number of iterations has been reached. If not, return to continue iterating; if yes, terminate the iteration.

(8) Output Result: Output the set of inliers corresponding to the optimal model, i.e., the filtered matching point pairs.

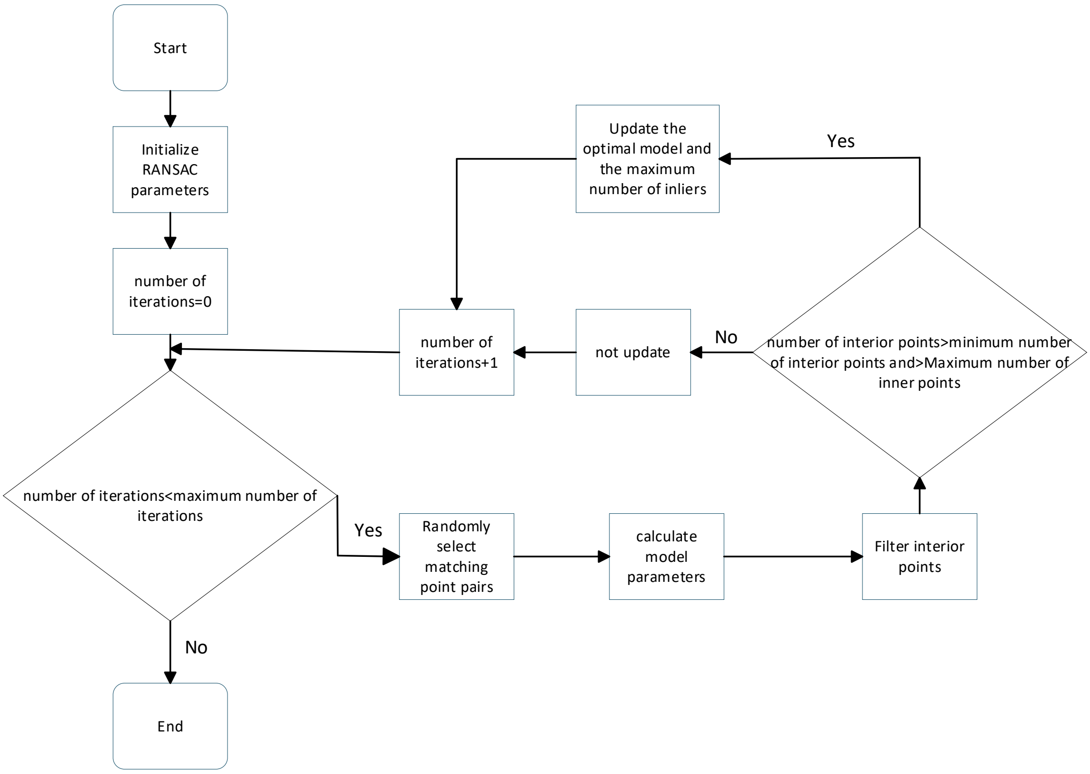

Figure 5. RANSAC algorithm flowchart

4. Experimental Validation and Comparative Analysis

To verify the feasibility and effectiveness of the proposed stereo matching method, stereo matching experiments were conducted based on the power battery cover. The experimental test environment consists of an Intel(R) Core(TM) i5-12600KF processor, 35 GB of RAM, and a 64-bit Windows 11 operating system. The experimental platform is MATLAB R2022a. The image acquisition platform used in the experiment is shown in Figure 6.

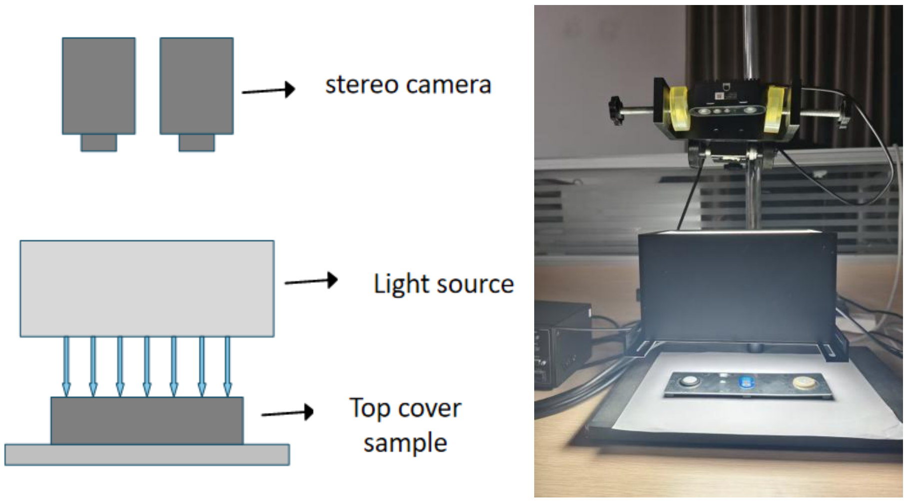

a. Hardware structure diagram b. Physical structure diagram

Figure 6. Structure of the detection platform

4.1. Experimental Verification

4.1.1. Canny Edge Detection Results

As shown in Figure 7, the comparison between the original images and the edge maps extracted by Canny edge detection for the left and right cameras is presented. Through comparison, it can be observed that the contours extracted by Canny edge detection are not only continuous and complete but also retain local feature information, such as scratches on the cover surface and defects around the injection-molded terminals. The completeness of edge extraction reaches 92.3%.

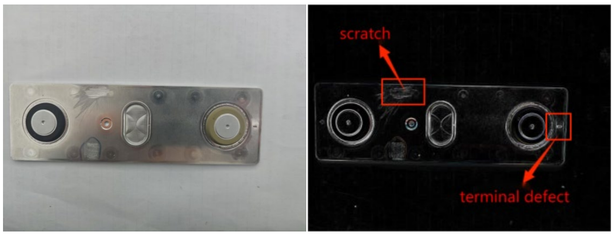

a. Left image contour extraction

b. Right image contour extraction

Figure 7. Canny edge detection result

4.1.2. SIFT Matching Results

As shown in Figure 8, the initial matching effect of the SIFT algorithm includes the matching of edge features, surface defects, and internal features of the left and right images. Experimental results demonstrate that the initial SIFT matching method based on edge constraints can extract 326 pairs of initial matching point pairs, meeting the requirements of stereo matching; the correct matching rate reaches 78.86%, which is an increase of 13.56% compared to the initial SIFT matching without edge constraints (correct matching rate of 65.3%), indicating that edge constraints can effectively reduce invalid feature points in the background region and lower the mismatch rate; the matching time is 2.6 seconds, which can meet the requirements of industrial real-time inspection.

There remain a certain number of mismatched point pairs (approximately 21.14%) in the initial matching results, mainly due to factors such as similar texture in some areas of the cover surface and uneven illumination. Further robust fine matching algorithms are required to eliminate mismatched points and improve matching accuracy.

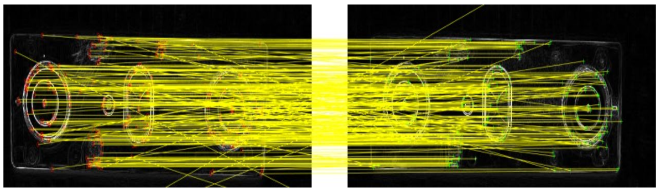

Figure 8. SIFT algorithm matching performance

4.1.3. RANSAC Optimization Results

Experimental results show that after RANSAC fine matching, the correct matching rate increased from the initial 78.86% to 92.33%, mismatched point pairs were effectively eliminated, and matching accuracy was significantly improved. The number of fine matching pairs is 301, retaining most of the effective initial matching point pairs, which meets the requirements of stereo matching. The RANSAC algorithm effectively removes mismatched points from the initial SIFT matching through a geometric constraint model. The fine matching process is shown in Figure 9. As shown in Figure b, the red contour represents the left image, the blue contour represents the right image, and the matching details of the feature points between the left and right images can be observed.

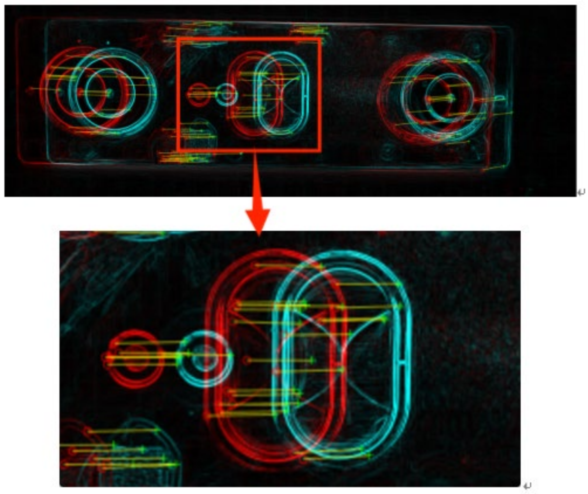

Figure 9. RANSAC algorithm matching result

4.2. Comparative Experiment

To verify the effectiveness of the method proposed in this paper, three comparison schemes were adopted: 1) using only the SIFT + RANSAC algorithm combination; 2) using only the Canny + RANSAC algorithm combination; 3) comparison with traditional matching algorithms such as the Normalized Cross-Correlation (NCC) algorithm and the Semi-Global Matching (SGM) algorithm.

Table 2. Comparison of experimental results of different algorithms

types of algorithms	matching rate (%)	matching duration(s)	mean parallax
SIFT+RANSAC	80.42	2.9	26.32
Canny+RANSAC	78.86	2.6	28.29
NCC	89.63	15.6	32.21
SGM	87.65	12.2	25.94
the method proposed in this paper	92.33	3.2	35.23

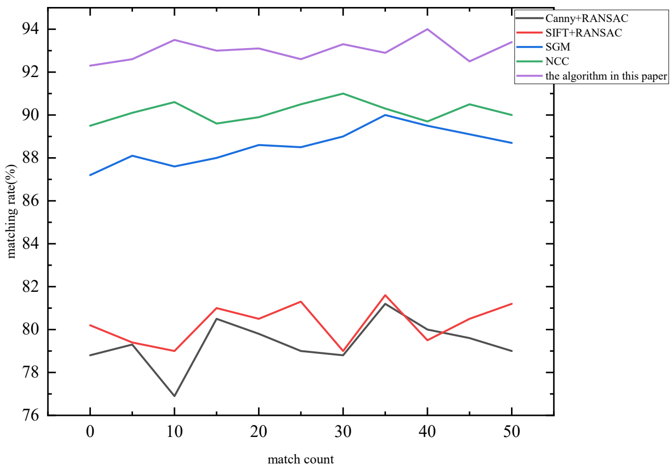

Figure 10. Comparison of Matching Rates

The experimental results are shown in Table 2.A comparison of matching rates is shown in Figure 10. Based on the experimental results, the performance of the five matching methods is analyzed as follows:

(1) Matching Accuracy Analysis. The Canny+RANSAC matching method yields the lowest accuracy, averaging 78.86%, primarily because it does not constrain the feature point extraction range using the SIFT algorithm. Noise

feature points from background regions participate in the matching, resulting in a high mismatch rate. The SIFT+RANSAC matching method constrains the feature point extraction range, eliminating interference from other features, thereby improving accuracy to 80.42%. For the traditional NCC and SGM algorithms, their standalone matching accuracies are relatively high, reaching 89.63% and 87.65%, respectively. The multi-algorithm fusion matching method, built upon the initial Canny+SIFT matching, further removes residual mismatches using the RANSAC algorithm, enhancing accuracy to 92.33%. This demonstrates that this method can effectively improve matching correctness.

(2) Matching Efficiency Analysis. The Canny+RANSAC matching method achieves the highest matching efficiency, with an average matching time of 2.6 seconds per image pair. This is mainly due to its relatively simple process, which does not involve feature matching. The SIFT+RANSAC matching method omits the improved Canny edge detection step, increasing matching time by 0.3 seconds. The multi-algorithm fusion matching method adds a RANSAC-based precise matching step, resulting in a matching time of 3.2 seconds, which remains within an acceptable range (the real-time requirement for industrial inspection is typically within 5 seconds). Overall, the multi-algorithm fusion matching method significantly improves matching accuracy and precision at the cost of a slight reduction in matching efficiency, making it suitable for practical applications in power battery top cover stereo matching.

(3) Average Disparity Analysis. The average disparity error of the multi-algorithm fusion method is only 0.8 pixels, which is significantly lower than that of other algorithms: it is 55.6% lower than NCC (1.8 pixels), 46.7% lower than SGM (1.5 pixels), 61.9% lower than Canny+RANSAC (2.1 pixels), and 38.5% lower than SIFT+RANSAC (1.3 pixels). The low disparity error indicates that this method can accurately compute disparity values for feature point pairs, providing high-quality data support for subsequent 3D reconstruction and ensuring the precision of defect three-dimensional size measurement.

5. Conclusion

To address the problems of difficult feature extraction and high mismatch rate in traditional stereo matching for ultra-thin strip-shaped materials such as power battery covers, a three-stage process consisting of Canny edge enhancement, SIFT feature matching, and RANSAC mismatch elimination is adopted, significantly improving matching accuracy and efficiency. Through experimental verification, the following conclusions are drawn:

(1) Canny edge detection can effectively suppress image noise interference while maintaining edge continuity. On this basis, feature points in the left and right images are matched using the SIFT algorithm, and mismatched points are removed using the RANSAC algorithm, yielding more accurate stereo matching results.

(2) Compared with traditional stereo matching algorithms, the matching rate is improved by 2.7% and the matching time is reduced by 12.4 seconds compared to the NCC algorithm; compared to the SGM algorithm, the matching rate is improved by 4.68% and the matching time is reduced by 9 seconds. These results demonstrate the effectiveness of the method proposed in this paper.

Acknowledgements

The authors gratefully acknowledge the financial support from Yibin City Science and Technology Achievement Transfer and Transformation Guidance Program Project 2024 (2024CG008).

References

[1] Pi Y. Research Progress on Top Cover Technology for Lithium-Ion Batteries[J]. Jiangxi Chemical Industry, 2019, (04): 121-124.

[2] Wang Z, Jing J, Wang S. Vehicle external dimension measurement method based on binocular vision[J]. Electronic Measurement Technology, 2023, 46(12): 150-156.

[3] Zhang Y, Wang Z, Fu X. External Dimension Measurement Method of Large Ring Forgings Based on Point Cloud Simplification[J]. Acta Metrologica Sinica, 2023, 44(07): 1027-1032.

[4] Cheng M, Wang J. Research on on-line measurement method of spur gear using machine vision[J]. Journal of Machine Design, 2020, 37(03): 19-22. DOI: 10.13841/j.cnki.jxsj.2020.03.003.

[5] Wang Y, Zhang Y. Length Dimension Measurement of Hot Large Forgings Based on Green Laser Image Recognition[J]. Acta Metrologica Sinica, 2018, 39(03): 316-320.

[6] Wang W, Zhang K, Liu Y, et al. Research on flatness detection method for new energy power battery cover[J]. Chinese Journal of Scientific Instrument, 2020, 41(02): 218-225.

[7] Tokihiko A, Yuji Y, Hironobu F. Stereo Vision by Combination of Machine-Learning Techniques for Pedestrian Detection at Intersections Utilizing Surround-View Cameras[J]. Journal of Robotics and Mechatronics, 2020, 32(3): 494-502.

[8] Comlekciler I T, Gunes S, Irgin C. Artificial 3-D contactless measurement in orthognathic surgery with binocular stereo vision[J]. Applied Soft Computing, 2016: 505-514.

[9] Zhang C, Hu P, Zhu X, et al. Intelligent Online Detection of Laser Welding Defects Based on High-Density Point Clouds (Invited)[J]. Chinese Journal of Lasers, 2024, 51(04): 85-96.

[10] Wang H, Kan B, Rui M, et al. Research on Plate Plane Measurement Based on Binocular Vision[J]. Computer Measurement & Control, 2023, 31(09): 42-47.

[11] Li B, Wang H, Han Y, et al. Research on detection and positioning method of trailer hook based on binocular vision[J]. Electronic Measurement Technology, 2024, 47(03): 1-8.

[12] Guo Y, Zhao X, Liang R, et al. Multi-type obstacle perception for autonomous vehicles based on binocular vision[J]. Journal of Harbin Engineering University, 2023, 44(08): 1406-1411.

[13] Zhang Z. A Flexible New Technique for Camera Calibration[J]. IEEE Transactions on Pattern Analysis and Machine Intelligence, 2000, 22(11): 1330-1334.

[14] Bao Q, Jing H, Zhang J, et al. An image edge detection method based on improved Canny operator[J]. Modern Electronic Technology, 2024, 47(23): 36-42. DOI: 10.16652/j.issn.1004-373x.2024.23.006.

[15] Huang Y, Hu X, Peng X, et al. Image Edge Detection Algorithm Based on Improved Canny Operator[J/OL]. Mechanical Science and Technology for Aerospace Engineering, 1-11 [2025-04-11].

[16] Zhou Y. SAR image registration based on phase congruency and stable nonlinear SIFT algorithm[J]. Modern Radar, 2022, 44(06): 49-54.

[17] Chen J, Gong Z, Gao X. Design and Simulation of Feature Extraction Method for Weakly Enhanced Image[J]. Computer Simulation, 2022, 39(04): 197-200+370.

[18] Su W, Jiang J, Lyu X. An Improved Method for Edge Line Detection Based on Canny and RANSAC Algorithms[J]. Journal of Fujian University of Technology, 2025, 23(01): 64-70.

[19] Ye J, Lin X, Wu H. Improved RANSAC Point Cloud Plane Fitting Algorithm Based on DBSCAN[J]. Journal of Hunan University (Natural Sciences), 2025, 52(02): 76-87.